Volume 16
Number 5
October 2020
Pages 401–504

Molecular Omics

rsc.li/molomics

ISSN 2515-4184

ROYAL SOCIETY OF CHEMISTRY

RESEARCH ARTICLE
Sanjoy K. Bhattacharya *et al.*
Aqueous humor metabolite profile of pseudoexfoliation glaucoma is distinctive

Indexed in Medline!

Molecular Omics

ROYAL SOCIETY OF CHEMISTRY

RESEARCH ARTICLE

View Article Online
View Journal | View Issue

Cite this: *Mol. Omics*, 2020, **16**, 425

Aqueous humor metabolite profile of pseudoexfoliation glaucoma is distinctive†

Ciara Myer,[ab] Leila Abdelrahman,[ab] Santanu Banerjee,[abc] Ram B. Khattri,[d] Matthew E. Merritt,[d] Anna K. Junk,[abe] Richard K. Lee[ab] and Sanjoy K. Bhattacharya*[ab]

Pseudoexfoliation (PEX) is a known cause of secondary open angle glaucoma. PEX glaucoma is associated with structural and metabolic changes in the eye. Despite similarities, PEX and primary open angle glaucoma (POAG) may have differences in the composition of metabolites. We analyzed the metabolites of the aqueous humor (AH) of PEX subjects sequentially first using nuclear magnetic resonance (^{1}H NMR: HSQC and TOCSY), and subsequently with liquid chromatography tandem mass spectrometry (LC-MS/MS) implementing isotopic ratio outlier analysis (IROA) quantification. The findings were compared with previous results for POAG and control subjects analyzed using identical sequential steps. We found significant differences in metabolites between the three conditions. Principle component analysis (PCA) and partial least squares discriminant analysis (PLS-DA) indicated clear grouping based on the metabolomes of the three conditions. We used machine learning algorithms and a percentage set of the data to train, and utilized a different or larger dataset to test whether a trained model can correctly classify the test dataset as PEX, POAG or control. Three different algorithms: linear support vector machines (SVM), deep learning, and a neural network were used for prediction. They all accurately classified the test datasets based on the AH metabolome of the sample. We next compared the AH metabolome with known AH and TM proteomes and genomes in order to understand metabolic pathways that may contribute to alterations in the AH metabolome in PEX. We found potential protein/gene pathways associated with observed significant metabolite changes in PEX.

Received 17th December 2019,
Accepted 23rd February 2020

DOI: 10.1039/c9mo00192a

rsc.li/molomics

Introduction

Pseudoexfoliation (PEX) is an age-related systemic syndrome. It is characterized by generalized fibrotic aberration of extracellular matrix. It is associated with the presence of PEX fluffy materials with ocular manifestation and glaucoma.[1,2] PEX is also associated with cardiovascular and cerebrovascular morbidity.[1] Although PEX has obvious ocular manifestations such as fluffy deposits on the crystalline lens and glaucoma, the underlying disease is systemic and can affect multiple organ systems (ESI†). Furthermore, PEX is not restricted to geographic boundaries and hence is of worldwide significance. Despite ocular effects and glaucoma, the material deposit is systemic.

The presence of pseudoexfoliation material identified by clinical examination at the slit lamp results in the diagnosis of PEX. It is thus a form of open angle glaucoma with a known etiology. Large aggregates of dandruff-like floating clumps of proteinaceous material circulate in the anterior chamber. The deposit material is evident on a slit lamp exam as a layer of white material on the lens capsule (LC) often giving a bull's eye-like configuration where the pupil excursion has mechanically rubbed of the deposits. Formation of this abnormal material in the anterior segment of the PEX eye results in several clinical and surgical ocular conditions including secondary open angle glaucoma, angle narrowing, an increased iris vascular leak, and zonular dehiscence associated with increased risk of lens nucleus prolapse during cataract surgery.[1] PEX material is believed to cause intraocular pressure (IOP) elevation by obstructing the trabecular meshwork and subsequently restricting the aqueous humor (AH) outflow, ultimately resulting in optic nerve damage. The source of the PEX material is not entirely certain and the molecular identity of the PEX material is not completely known. The fibrillar protein aggregates have been hypothesized to originate from the cells of the iris, the lens, and the ciliary epithelium by various groups.[1,3]

PEX has a genetic predisposition. Inheritance of PEX has been found to be an autosomal dominant trait. However, mutations associated with PEX also result in late onset and incomplete

[a] *Bascom Palmer Eye Institute, University of Miami, Miami, Florida, USA. E-mail: sbhattacharya@med.miami.edu*
[b] *Miami Integrative Metabolomics Research Center, University of Miami, Miami, Florida, USA*
[c] *Department of Surgery, University of Miami, Miami, Florida, USA*
[d] *University of Florida, Gainesville, Florida, USA*
[e] *Miami Veterans Affairs Healthcare System, Miami, Florida, USA*

† Electronic supplementary information (ESI) available. See DOI: 10.1039/c9mo00192a

penetrance.[4] Incomplete penetrance, the widely used term in genetics,[5] refers here a situation where a known gene mutation demonstrate varied degree of disease severity in different individuals. Thus, like several other late onset, progressive and complex ocular diseases, PEX is clinically and genetically heterogeneous. PEX has been associated with a maternal[6,7] as well as a paternal transmission.[8] In addition, it has been associated with transmission in two-generation families, higher concordance rates in monozygous twins, familial aggregation of patients, increased risk in relatives, loss of heterozygosity support and genetic predisposition.[6,9] The development of PEX occurs not at the same rate and time bilaterally, thus it presents asymmetric involvement. Regional clustering observed in PEX patients also suggests genetic predisposition as well as potential involvement of climatic factors.[10–12]

PEX occurs in all geographic regions worldwide with varying prevalence rates.[13] One of the early epidemiologic studies found a lack of influence of climate on the occurrence of PEX syndrome.[4] Recent studies suggest that climatic factors affect PEX.[12,14] Greater time spent outdoors during the summer up to age 24[15] or over a lifetime[16] has been found independently associated with greater risk of incident PEX. Thus, outdoor climatic factors are considered an independent risk for the development of PEX. Increased incidence of cataracts suggests involvement of ultraviolet light.[16]

There is reduced protection from ultraviolet light due to reduced levels of ascorbic acid in the AH of PEX. Metabolites such as homocysteine, folic acid vitamin B12, and many other metabolites are possibly associated with glaucoma.[17–21] However, these individual studies of metabolites have often produced conflicting results.[22] Several proteomic studies and genomic studies on PEX have been reported.[23–25] Proteomic studies have shown elevated level of vitamin D binding protein. Increased vitamin D and vitamin D binding protein are known to correlate with elevated sunlight exposure. In contrast to several proteomic and genomic studies, high throughput investigations of metabolite profiles of PEX tissue and fluids are lacking, despite individual studies of selected metabolites. AH metabolites changes may potentially herald the transition from normal to pathologic state. Metabolomic analysis of AH in PEX and comparison with control normal AH will provide insight into the pathophysiologic metabolic changes in the anterior chamber.

Results

Metabolite identification

We identified a total of 298 metabolites in pseudoexfoliation (PEX) glaucoma, primary open angle glaucoma (POAG) and non-glaucomatous controls using both one-dimensional (1D) ^{1}H NMR and isotopic ratio outlier analysis (IROA) (Fig. 1). The metabolites with their corresponding chemical shifts are shown in Fig. S2a–c and S3–S5 (ESI†). 1D ^{1}H NMR identified metabolites were verified further with the 2D NMR spectra: HSQC and TOCSY shown in Fig. S6–S8 (ESI†). Within the total number of metabolites identified there were 125 unique PEX, 63 unique POAG and 100 common metabolites. IROA identified

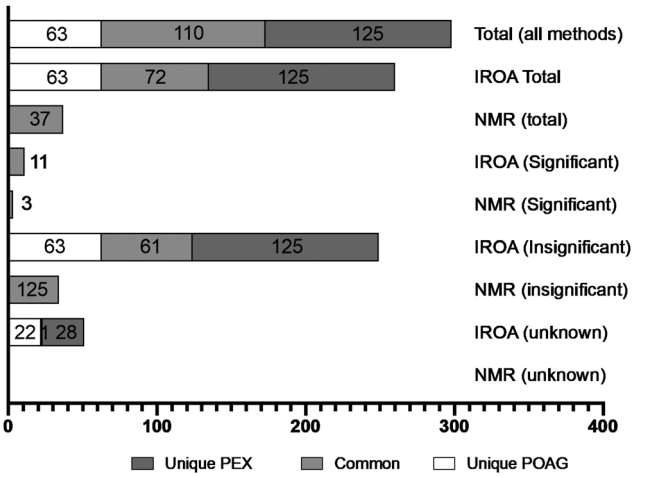

Fig. 1 A summary of the number of metabolites identified in control, pseudoexfoliation (PEX) and primary open angle (POAG) glaucoma samples. The combined metabolites identified using ^{1}H NMR and isotopic ratio outlier (IROA) mass spectrometric analysis have been presented. Bar plots indicate the intersections of the different metabolites discovered for the control, POAG and PEX glaucoma. Summary of all metabolites have been presented. Significant metabolites are those which have shown a p value ≤ 0.05.

a total of 125 and 63 metabolites in PEX and POAG respectively and 72 metabolites in common between the groups. ^{1}H NMR identified a total of 37 metabolites that were common among all AH groups (Fig. 1). A comparison of the resonances for a few metabolites for control (Normal), POAG and PEX samples is shown in Fig. S3–S5 (ESI†).

Comparison of PEX AH metabolites with POAG AH and control AH

There were 11 significant metabolites identified when comparing PEX to controls including L-arginine, L-lysine, L-glutamine, L-tyrosine, 2,4-diacetamido-2,4,6-trideoxy-beta-l-altrose, *N*(6)-acetonyllysine, 1-aminocyclopropane-1-carboxylate, L-histidine, C6H9N4O3P, C6H13NO9, and 5 hydroxypentanoate (Fig. 2a). Only 2 metabolites (propylene glycol, creatine) were found to be significant between PEX and controls using ^{1}H NMR spectroscopy (Fig. 2b). There were five amino acids (L-arginine, L-lysine, L-tyrosine, L-glutamine, L-histidine) that showed varying levels when comparing PEX, POAG, and control (Fig. 2). The amino acid levels were greater in POAG compared to PEX in IROA (Fig. 2c), and higher in controls compared to PEX (Fig. 2a). ^{1}H NMR analysis revealed that 2-hydroxybutyrate, 3-methyl-2-oxovalerate, propylene glycol, 3-hydroxy isovalerate, pyruvate, and choline had lower abundance in PEX compared to POAG (Fig. 2d).

Statistical analysis

The identified metabolites were subjected to principle component analysis (PCA), partial least square-discriminant (PLS-DA) and variable importance in projection (VIP) score analysis. PCA and PLS-DA distinguished PEX metabolites from control and PEX from POAG metabolites (Fig. 3). The VIP score presented several important metabolites that showed differential levels in PEX compared to control (Fig. 3c). Similarly, VIP scores presented several important metabolites that showed differential levels in

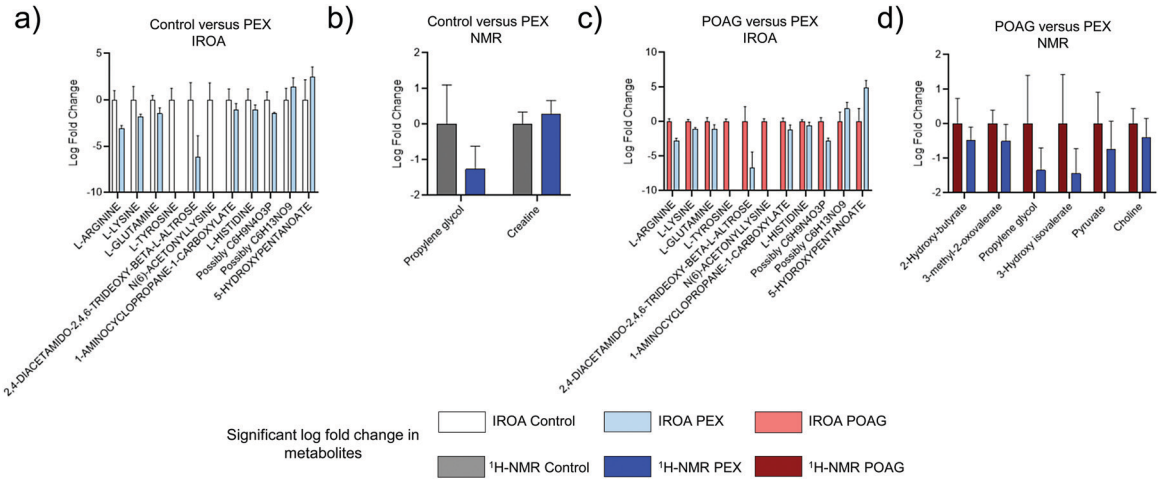

Fig. 2 The significant metabolites found in control, PEX and POAG using NMR or IROA methods as indicated. (a) IROA significant metabolites for control *versus* PEX. (b) ^{1}H NMR significant metabolites for control *versus* PEX. (c) IROA significant metabolites for PEX *versus* POAG. (d) ^{1}H NMR significant metabolites for PEX *versus* POAG.

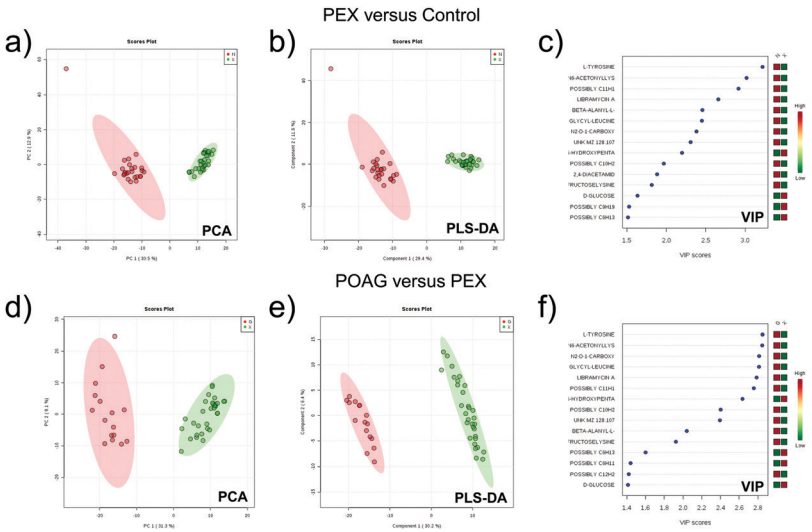

Fig. 3 The statistical analysis of metabolites in control, PEX and POAG AH samples. (a and d) The principal component analysis (PCA), (b and e) partial least squares discriminant analysis (PLS-DA) and (c and f) variable importance in projection (VIP) scores for the combined ^{1}H NMR and IROA data. A two-component analysis (PC1 *versus* PC2) was determined for PEX *versus* control and POAG *versus* PEX. Control, POAG and PEX are indicated by N, X and G respectively. All determinations were made using MetaboAnalyst 4.0 web-based tools.

PEX compared to POAG (Fig. 3e). The VIP score also presented several important metabolites used to classify samples as either POAG or PEX (Fig. 3f). It is noteworthy that certain significantly abundant ($p < 0.05$) metabolites like L-tyrosine and *N*6-acetonyllysine also had the highest VIP scores in both experiments. The PLS-DA Q2 score for the PEX *versus* control experiments was 0.95 for the first principal component and was 0.94 for the second principal component. For comparison of PEX and control, the PLS-DA Q2 score was 0.95 for the first principal component and 0.98 for the second principal component. These extremely high Q2 scores indicate that the model is highly predictive in classifying control, PEX, and POAG samples based on metabolites. Volcano plots were created to identify significant metabolites. They showed the presence of distinct finger-print regions of abundance for POAG, PEX, and control (Fig. 4). These plots confirm the accuracy of the PLS-DA model in classifying the conditions. Heat maps were constructed to compare the metabolites of control *versus* PEX (Fig. 5a) and POAG *versus* PEX (Fig. 5b). Clustering of certain over abundant and under abundant metabolites mapped to either control, POAG, or PEX.

Predictive power of metabolite datasets

We tested whether metabolomic profiles of control, POAG and PEX can be used to classify and distinguish the conditions (Fig. 6). We used machine learning to create an enhanced neural network, support vector machine (SVM) and deep learning algorithm. The enhanced neural network showed that training on only 10% of the whole patient samples, while testing on the remaining 90% (or 100 − x% where x is the training set percent; x represents the combination of samples from whole metabolites of individual

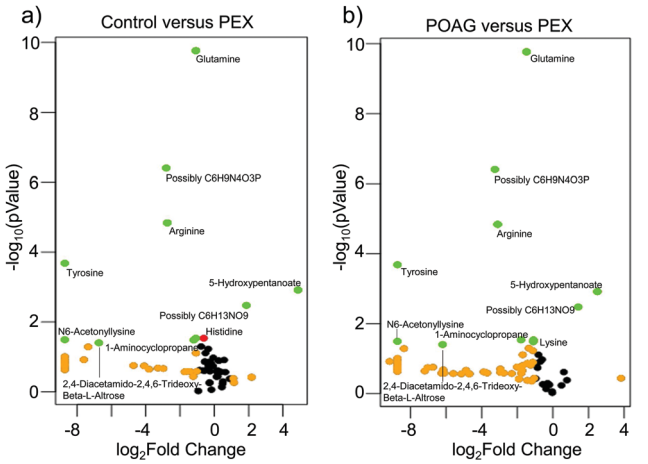

Fig. 4 Volcano plots comparing the significance of the metabolites found ($\log_{10} p$) *vs.* the $\log_2$ fold change. (a) Control *versus* PEX experiments. (b) POAG *versus* PEX experiments. Metabolites in green had a significant difference in expression ($p < 0.05$) and a magnitude $\log_2$ fold change greater than 1. Metabolites in orange did not have a significant difference in expression but did have a magnitude $\log_2$ fold change greater than 1. Metabolites in red only had a significant difference in expression. Black metabolites neither had a significant difference in expression nor a magnitude $\log_2$ fold change greater than 1. Metabolites in green are labeled.

patients) of the samples, can lead to greater than 90% accuracy in classifying PEX and control samples (Fig. 6a) or PEX and POAG samples (Fig. 6b). Deep learning was next best for either classification. We found the SVM algorithm to be unpredictable in predicting either group (Fig. 6a and b) as its output did not show a linear relationship with the input dataset.

Metabolite interactor protein network

We combined the identified metabolites in this study with prior quantitative proteomics[26] and genomics data[27] towards building an integrated metabolite–protein–genome network that can provide important hubs of convergence of these biomolecules (Fig. 7). We used the difference in relative abundance levels of metabolites in PEX compared to control towards building this network. There were four prominent metabolite nodes included L-tyrosine, L-lysine, L-histidine, and L-arginine. These same nodes were also confirmed as significant metabolites in our experiments. The prominent hubs of convergence bear potential to test specific hypotheses. L-Arginine, related to NO generation and L-tyrosine metabolism are pertinent to IOP homeostasis and TM integrity respectively[28,29] underscoring the importance of these nodes.

Discussion

For more than two centuries AH was considered as a static fluid, something that people are born with,[30] experimental investigation within the last five decades showed AH as an active product of the ciliary body[31–34] and helped evolve the

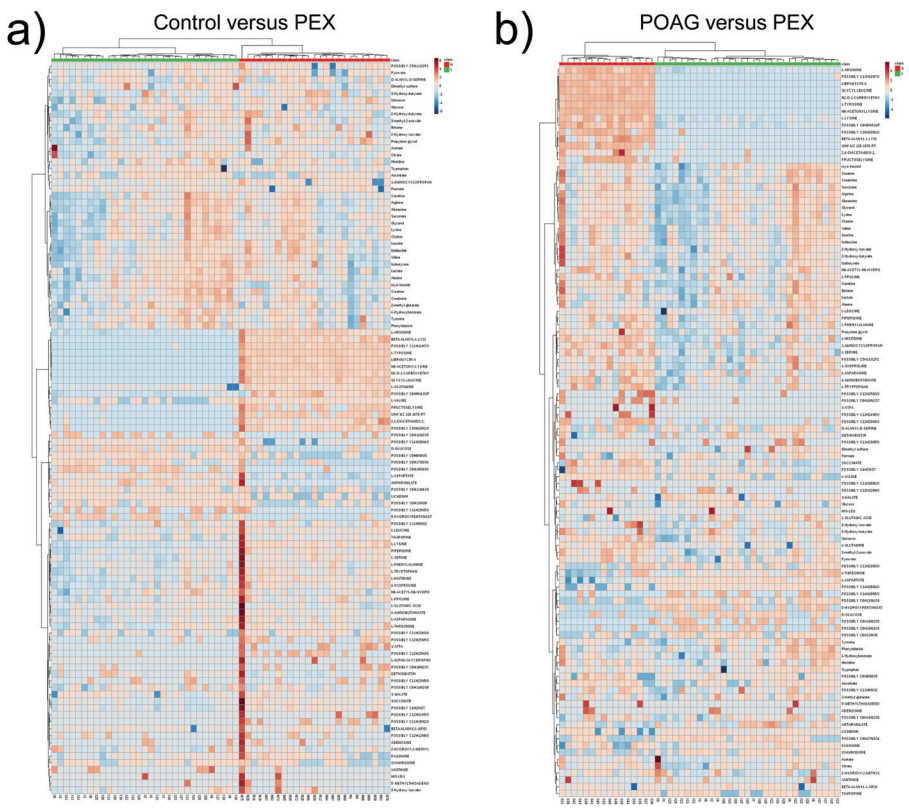

Fig. 5 Heat maps of metabolites. ^{1}H NMR and IROA combined data were used to generate heat-maps. (a) ^{1}H NMR and IROA significant ($p < 0.05$) and insignificant metabolites including unknowns for control *versus* PEX. (b) ^{1}H NMR and IROA significant ($p < 0.05$) and insignificant metabolites including unknowns for the POAG *versus* PEX experiments. The *x*-axis represents class and the *y*-axis represents metabolites.

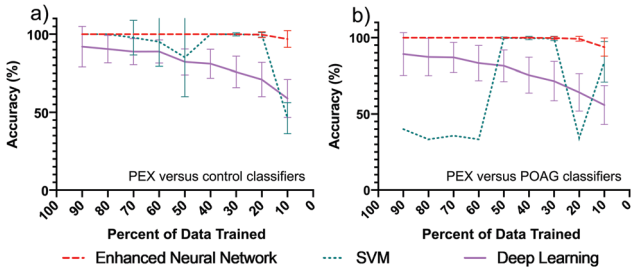

Fig. 6 Classification of samples as control, POAG or PEX based on metabolite profiles using machine-learning. (a) The accuracy rates of the three different models explored machine learning algorithm as a function of percent data trained for the PEX *versus* control. (b) The accuracy rates of the three different explored machine learning algorithms as a function of percent data trained for the PEX *versus* POAG experiments. The high variability of the linear SVM could be due to the use of a linear kernel indicating the limitations of use of linear kernel in standard software setting. The *x*-axis shows the percentage of the data (10–100%) that was used for training. Combined refers to IROA plus ^{1}H NMR identified metabolites. A hundred iterations of a percentage-split validation of each algorithm was performed and the average accuracy [accuracy (%), output in *y*-axis], along with the standard deviation, of each percent trained data was plotted. Classification/prediction for each test used 100 − *x*% of the whole patient samples, where x represents the percentage of data used for training.

concept of AH as a dynamic fluid. However, it is highly likely that the metabolites of the AH are contributed by several different tissues of the anterior segment such as the cornea, lens, ciliary body, iris and uveosclera.[35] Several metabolites have been proposed to be present in the AH in individual analysis,[36] but may not be supported by high throughput metabolomics. AH outflow is likely to generate local turbulence, create a gradient between generation and exit streams and thus have an effect on the metabolite concentration.[37,38] The local turbulence in the AH outflow could be due to the TM pulsatile motion[39,40] as well as high hydraulic conductivity. The hydraulic conductivity of the aqueous humor pathway, is one of the highest of all filtration tissues (4000–9000 $\times$ 10^{-11} cm^2 s g^{-1}), including the renal filtration system.[41]

We identified 298 metabolites using combined methods of NMR and IROA. Currently, there is no report on PEX metabolites. The control and POAG AH have previously been subjected to metabolite analysis by various methods. Previous reports have used only one analytical method (such as mass spectrometry or routine biochemical analysis) at a time. However, we present data generated by a non-destructive ^{1}H NMR followed by a destructive IROA mass spectrometry, unlike most previous reports which utilized only destructive methods for metabolite identification. Many metabolites identified by our analysis are consistent with a recent spatial analysis using imaging mass spectrometry.[42]

A comparison of non-amino acid, non-lipid metabolites showed asymmetric dimethyl arginine (ADMA) to be present in higher levels in PEX compared to control (Fig. 3d). This is corroborated by prior reports.[43] Perhaps L-arginine is converted to ADMA in PEX. Compared to the POAG aqueous humor, 5-hydroxypentanoate was significantly higher in the PEX samples. This metabolite was also significantly elevated in PEX in comparison to the controls (Fig. 3d).

It is becoming increasingly evident that a single gene mutation may have different fates. Geneticist termed this as an incomplete penetrance. Investigations in isogenic organisms have expanded this understanding that a single mutation in a protein product derives different fates due to differences in interactions with other molecules, most commonly with metabolites.[44] Differential metabolites interacting with proteins have been shown in Fig. 7. In the future, detail and curated interaction maps will shed new light into protein–metabolite interactions in control *versus* disease states.

The neural network analysis algorithm of Rapidminer™ showed the best classification of AH into control, POAG and PXE categories even when training was done with as little as 10% of the total dataset. Our results using deep learning showed lack of predictability based on metabolite profiling compared to neuronal network (Fig. 6a and b). Deep learning, while it may have more hidden layers, is often prone to overfitting errors, and this may explain its decreased accuracy in classifying the conditions based on the metabolite abundance. Overfitting errors occur when a model has high training accuracy and can classify well on previously "seen" data, but when presented with new test data, the model has lower accuracy as it is not generalizable. The SVM model showed strange predictability, with varying accuracies at different percentages of data trained (Fig. 6a and b). The model's lack of robustness may have been due to training/testing on bad splits. RapidMiner utilized the "automatic" split ratio algorithm whereby samples were randomly selected during each split, while maintaining the original PEX: control ratio or POAG : PEX ratio. Perhaps due to this, the SVM encountered bad splits that affected test accuracy. Overfitting may have also affected performance.[45] Strategies to avoid overfitting include feature selection, maybe using only significant ($p < 0.05$) metabolites as our training features, and increasing the number of samples.

Our generated metabolite interactor network indicates distinct relationships between distinct proteins identified previously in the PEX materials and their metabolites. For example, TGM2, which catalyzes the crosslinking of proteins by epsilon-gamma glutamyl lysine isopeptide bonds has been shown to be upregulated in PEX.[26] Higher levels of TGM2 are expected to be negatively correlated with glutamine levels, which has been confirmed in our analysis (Fig. 2c). PEX has also been shown to be associated with oxidative stress.[22] The downregulation of MGST1, a protein associated with oxidative stress protection, correlates with the lower tyrosine levels in PEX, which was confirmed in our studies (Fig. 2) and illustrated in our network (Fig. 7). Other proteins, while not directly associated with PEX, have been detected in the generated network. Many such proteins for example, NOS3, have been implicated to play a role in POAG. NOS3 is involved in the conversion of L-arginine to generate nitric oxide[46] and is likely to play a role both in POAG and PEX induced glaucoma. Prior literature has shown that signs of PEX syndrome, such as fibrils manifestation, often appear later in eyes that were diagnosed as having PEX induced glaucoma.[1] Future investigations will elucidate if a correlation of the metabolite concentration exists with expression levels of specific proteins.

Environmental factors influence the metabolites. In human skin, 7-dehydrocholesterol is converted to vitamin D by the

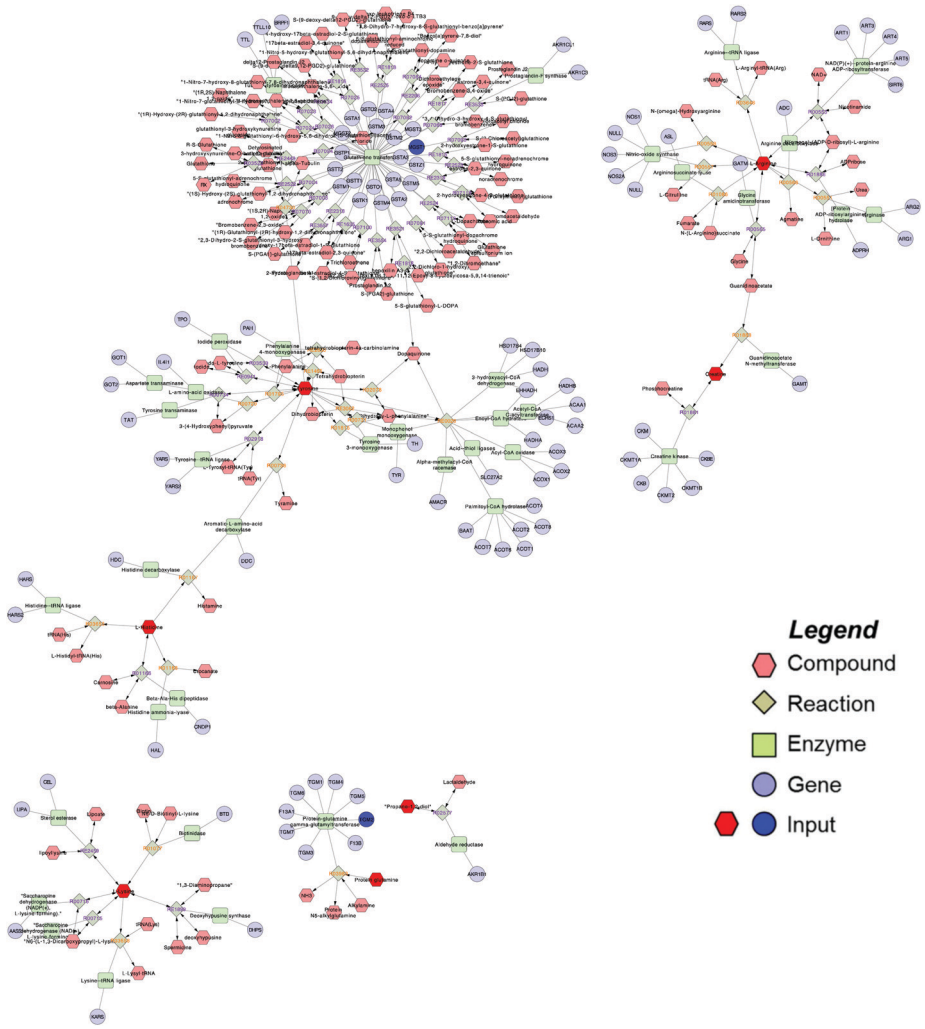

Fig. 7 Metabolite–protein–gene network of PEX as compared to control samples. Genes from the literature search are shown in dark blue. The input metabolites from this study are shown in dark red. Hubs in the network characterized by many edges surrounding a node indicate important sites for further future investigations. An interactive version of the network can be viewed by uploading the GRAPHML file into OmicsNet.ca or Cytoscape (ESI†).

ultraviolet B (UVB) radiation from solar radiation.[47] Vitamin D and other metabolite changes have been found in the cornea subjected to UVB present in the solar light.[48–50] Vitamin D binding protein has been identified as a constitutive protein of the AH,[51] and at increased level in PEX AH by mass spectrometry.[52–54] Altered levels of vitamin D and vitamin D binding protein are consistent with the hypothesis that environmental factors, especially UV light, affect an eye pre-disposed to PEX glaucoma.[12,14] Cold, heat and other environmental conditions also contribute to the metabolite composition in the AH. Eyes with glaucoma in general undergo tremendous diurnal fluctuation in intraocular pressure (IOP). The AH turnover and the alteration of the outflow facility has been recorded in glaucoma. The metabolite composition may vary due to the contribution of different tissues in the anterior eye segment for the AH. However, overall our results suggests that despite small variations due to different collection times and asynchrony with collection, machine-learning is able to correctly classify the groups as control, POAG and PEX even with as little as 10–20% of total samples or the data which has been generated using just 10–20 individuals in each group. The markers for glaucoma and PEX glaucoma in particular are useful predictors of susceptibility, rate of progression or efficacy of a given treatment.[55] With respect to PEX, the presentation of glaucoma and the deposit material is often asymmetric with the eye presenting the manifestation first.

The efficacy of bodily fluids, perspiration[56] and serum metabolites[57] have been recognized in identifying early stage damage or for accurate diagnosis of certain conditions utilizing machine-learning of metabolomics profiles. Targeted metabolites have been helpful in predicting difficult to predict entities including systemic and autoimmune diseases.[58] Future use of machine learning and metabolomics profiles may enable classification of primary open angle glaucoma into thus far unrecognized subtypes. AH *versus* the blood metabolome can be evaluated to investigate whether both provide the same subtype classification with different accuracies. As noted, such profiles may enable the prediction of susceptibility, progression and drug efficacy. Prediction of subtype and efficacy may move us one step closer

towards individualized medicine. Perhaps in the future complex stratification of glaucoma patients into different group and population-based targeting of susceptible or fast progression rate individuals will be also possible. The approaches for PEX described here is highly likely to be also applicable for systemic diseases as well.

In the future, a comparison of serum metabolites could be compared for the three distinct types of glaucoma and machine learning could be used to test the predictability into three groups accurately. They could also be compared with the AH metabolite profiles. Theoretically, it will be preferable to collect AH from both eyes of the patients that present monocular PEX and the binocular deposit formation delay. This could then be used for the prediction of the length of time for which the delay is observed and also perhaps for the disease severity. Due to the lack of sufficient treatment or medical reasons, paracentesis in the unaffected PEX eye is unlikely to be permit on institutional review. However, availability of PEX animals models[59] may enable rigorous testing of the AH, allow for collection of blood for comparison as well as machine-learning classification/prediction. A rigorous prediction capability will be a potential convincing argument for pilot test cases with human subjects. Serum metabolite-based diagnosis, prediction of susceptibility and severity in progression will be warranted modalities as tools in healthcare of potential disease subjects.

Methods

Human subjects and chemicals

All materials were collected from human donors without identifiers under institutional review board exemption and approval. We acquired 31 pseudoexfoliation (PEX) glaucomatous aqueous humor (AH) samples (see Table S1, ESI†) from participants at the University of Miami Bascom Palmer Eye Institute (Miami, FL). The primary open angle glaucoma (POAG) (n = 16) and non-glaucomatous controls (n = 25) previously analyzed were collected from the Veterans Affairs Healthcare System (VA) (Miami, FL). AH samples were used for ^{1}H-nuclear magnetic resonance (NMR) and subsequent isotopic ratio outlier analysis (IROA). Deuterated water (D_2O), and *D*6-4,4-dimethyl-4-silapentane-1-sulfonic acid (DSS) were obtained from Cambridge Isotope Laboratories, MA, USA. Monobasic and dibasic sodium phosphates, ethylene diamine tetracetic acid (EDTA) and sodium azide (NaN_3) were purchased from Sigma Aldrich, St Louis, MO, USA.

NMR spectroscopy

The nuclear magnetic resonance (NMR) spectroscopy experiments were performed at the Southeast Center for Integrated Metabolomics (SECIM), University of Florida (Gainesville, FL). AH samples were centrifuged at 13 200 rpm for 30 minutes at 4 °C, without any extraction. Fifty μL NMR samples were prepared by using 45 μL of the resulting supernatant of humor sample with 5 μL of Chenomx standard (Chenomx, Inc., Alberta, Canada) in D_2O, resulting in a final concentration of DSS of 0.5 mM. The sample was again centrifuged for 15 minutes at 13 200 rpm at 4 °C prior to loading the supernatant portion into 1.7 mm NMR tube. A 14.1 T Bruker NMR system with Avance Neo console and 1.7 mm TCl CryoProbe (Bruker BioSpin Corporation, Billerica, MA) was used to collect all 1D and 2D NMR spectra. Most of the 1D ^{1}H spectra were acquired with a first slice of NOESY pulse sequence.[60] For the spectra collected with the first slice of NOESY pulse sequence, 64 scans (nt) were collected along the 7142.9 Hz spectral width (sw) with 65 536 data points. A repetition time (Tr) of 5 s (1 s of relaxation delay (d1) and 4 s of acquisition time (at)) was used with a mixing time of 100 ms. 1D ^{1}H spectra for a few samples were acquired using zgpurge gprefocus4 pulse sequence[61] with the following parameters: ''d1'' of 2 s, ''nt'' of 256, sw of 9615.4 Hz, ''at'' of 1.42 s and 65 536 data points. For both types of experiments, pre-saturation of the water signal was obtained by low power radiation on resonance for water (during d1). Verification of the metabolite assignments were done by collecting Heteronuclear Single Quantum Coherence (HSQC) and Total Correlated Spectroscopy (TOCSY) spectra for one of the AH sample (N4). For the HSQC experiment, ''d1'' of 1.5 s, ''nt'' of 64, ''sw'' of 7211.5 Hz in f2-dimension and 24875.6 Hz in f1 dimension, and ''at'' of 0.3 s was used with GARP4 ^{13}C decoupling. The TOCSY experiment was collected with ''d1'' of 2 s, 16 scans, ''sweepwidth'' of 7211.5 Hz in both dimensions, and ''acquisition time'' of 0.3 s. MestReNova 14.0.1–23559 (Mestrelab Research, S.L., Santiago de Compostela, Spain) software was employed to process all NMR spectra. All ^{1}H free induction decays were exponentially line-broadened to 0.22 Hz, Fourier transformed, phased, base-line corrected (Spline method) and calibrated to internal reference (DSS) resonance at 0.0 ppm. Integrated areas for the preferred metabolites were extracted after normalizing all spectra with respect to DSS signal. Concentrations for those selected metabolites were determined using the extracted integrated areas and utilized for further metabolomics analysis. The NMR raw data for the control and POAG samples was uploaded to Metabolomics Workbench under study ID ST001285. The raw data for the PEX samples was uploaded to the same database under study ID ST001284.

Isotopic ratio outlier analysis (IROA)

Following NMR spectroscopy, the 31 PEX samples were prepared for isotopic ratio outlier analysis (IROA). The 50 μL of aqueous humor (AH) was combined with 800 μL of precipitate solution (8 : 1 : 1 acetonitrile : methanol : acetone). The metabolites were vortexed, incubated at 4 °C for 30 minutes, and subsequently incubated at −20 °C for 1 hour. Each AH sample was centrifuged at 20 000 × g for 10 minutes at 4 °C to form a pellet and 375 μL of supernatant was collected. The supernatant was dried in a speed vacuum for 20 minutes or until the sample was fully dry and stored at −20 °C until analysis by liquid chromatography tandem mass spectrometry (LC-MS/MS). Prior to LC-MS/MS, the IROA internal standard (IROA-IS, IROA technologies) (U-95% 13C) was reconstituted in 1.2 mL of LC-MS grade water with 0.1% formic acid (FA). The samples were reconstituted in 25 μL of LC-MS grade water with 0.1% FA and 10 μL was combined with 20 μL of IROA-IS. A long-term reference standard (LTRS) was reconstituted in 50 μL of

LC-MS grade water with 0.1% FA and subjected to LC-MS/MS as the first, last, and every 10th sample. Metabolite identification and relative quantification were performed using Clusterfinder Build 3.1.10 (IROA Technologies). Thermo raw files were converted into mzxml files before importation into the Clusterfinder software. The manufacturer protocols were followed to recognize IROA peak pairs and determine molecular formulas. Metabolites were identified by comparing retention time, molecular formula and molecular ion *m*/*z* with the Mass Spectrometry Metabolite Library of Standards (MSMLS, IROA technologies). Both, primary open angle (POAG) and control samples were analyzed utilizing the same methodology as previously described. To quantify metabolite abundance, the IROA C12 : C13 ratio was used. These results were used in the subsequent bioinformatics analysis. The raw data in the form of Thermo RAW files for each sample were uploaded to Metabolomics Workbench under study ID ST001278 for the control and POAG samples and study ID ST001277 for the PEX samples. The mwTAB files also include the mass to charge ratios and retention times of the metabolites found in each sample with their respective C12 : C13 ratios in both positive and negative ion mode.

High performance liquid chromatography (HPLC) – mass spectrometry

Reversed-phase chromatographic separation utilized an Accela autosampler, an Accela 600 pump (Thermo) and an ACE Excel 2 C18-PFP (100 × 2.1 mm, 2 μm) column. The solvents were LC-MS grade water with 0.1% formic acid (FA) and LC-MS grade acetonitrile with 0.1% FA as solvent A and solvent B respectively. The flow rate was 350 μL min^{-1} and the injection volume was 5 μL. The column temperature and tray temperature were 40 °C and 4 °C respectively. The gradient was 0–40% solvent B over 10 minutes, 40% solvent B over 10–12 minutes, 60% solvent B over 12–14 minutes, 95% solvent B over 14–20 minutes, 0% solvent B over 20–27 minutes, 0% solvent B was held for 27–30 minutes. The metabolites were analyzed using a Q Exactive Mass Spectrometer (Thermo) equipped with a heated electrospray ionization source (HESI) operating in both positive and negative ion modes. The HESI source operated at a spray voltage of 4 kV, a HESI vaporization temperature of 300 °C, and a heated capillary temperature of 325 °C and 310 °C for positive and negative ionization modes respectively. The sheath gas flow rate was 45 (negative mode) and 40 (positive mode). The auxiliary gas flow rate was 10 (negative mode) and 5 (positive mode). The S-lens radio frequency (RF) level was set to 30. Full scan was used with a mass range of 70–800 *m*/*z* with a resolution of 70 000, automatic gain control (AGC) target of 1×10^6, and maximum injection time (IT) of 100 ms. Data-dependent MS/MS used a loop count of 10, resolution of 17 500, AGC target of 5×10^2, maximum IT of 50 ms, isolation window of 2 *m*/*z*, and collision energy of 30.

Statistical analysis

Analyses were conducted using MetaboAnalyst 4.0, GraphPad Prism 8.2.1, Cytoscape 3.6.1 and MetScape 3.1.3. For the principal component analysis (PCA), partial least squares discriminant analysis (PLS-DA), and heat maps, the data was normalized against the metabolites of the control samples to find the fold change. The PEX metabolites were also normalized against the metabolites from the POAG samples. Mean fold changes and standard deviation were calculated, and significance was determined by a two-tailed, independent samples *t*-test. The samples were assumed to have equal variance, as the assumption of homogeneity of variances was used between the two sample groups. The normalized results were fed into Metaboanalyst and $\log_2$ transformed to ensure a normal distribution of metabolites (Chong *et al.*, 2018). The significant metabolite $\log_2$ fold changes were plotted for PEX *versus* control and PEX *versus* POAG in GraphPad Prism. Significant differentially expressed proteins found in the PEX aqueous humor (AH), and the PEX material itself,[26] were used with a list of genes associated with PEX[27] for pathway analysis. For the proteins and genes, Entrez ID numbers (corresponding to accession numbers in the UniProt database) were used. For the metabolites, the Kyoto encyclopedia of genes and genome or KEGG IDs (KEGG Compound Database) corresponding to compound names were used. The Entrez and KEGG IDs were fed into the MetsScape interaction network generator in Cytoscape to construct networks showing the protein–protein and protein–metabolite interactions as done in a previously published study.[62]

Machine learning

The RapidMiner™ 9.4 software was used to train computer algorithms with metabolomes of PEX and POAG to classify unknown metabolome profiles as each respective condition. Fig. S1 represents a workflow for data processing that was built to use split-validation model training and testing on various metabolome profiles (ESI†). The three RapidMiner algorithms examined were Support Vector Machine (SVM), an Improved Neural Network, and Deep Learning. SVMs with binary classification plotted the location of each point in a hyper-space (a multidimensional space). Using gradient descent, the algorithm then drew an optimized hyperplane maximizing the distinction between the two classes. This hyperplane was used for the training data set and was subsequently applied to the test set to predict the class of unknown samples based on their metabolite profiles. The neural networks optimized learning through feed-forward and back-propagation. A program we named "Gradient Training" was devised to set up a gradient of the percentage of data trained for each of the models, and the accuracy of classification as either PEX, Control, or POAG for each model was logged. One hundred iterations of this procedure were performed for each algorithm. The average accuracies, along with standard deviations, of correct classification for PEX *versus* control and POAG *versus* PEX samples were plotted in GraphPad Prism. For the "Gradient Training" program, an XML file is included in the ESI.† This XML file can be uploaded into RapidMiner™ and can be modified or tailored for specified analyses as needed.

Conclusions

We identified a total of 235 metabolites in the PEX AH. Several of these has been found in previous individual analysis in the past.

The machine-learning accurately classified AH into control, POAG and PEX groups based on the metabolite profiles. The metabolite profiles present opportunity for future prediction of susceptibility, rate of progression and drug efficacy.

Conflicts of interest

There are no conflicts to declare.

Acknowledgements

The funding support for this study was partly provided by a grant from Glaucoma Foundation of New York, NIH grant EY14801 and an unrestricted grant from Research to Prevent Blindness. The NMR study was partly performed at Southeast Center for Integrated Metabolomics, supported by NIH award U24DK097209 and partly at the National High Magnetic Field Laboratory, supported by National Science Foundation Cooperative Agreement No. DMR-1644779 and the State of Florida. Metabolomics workbench is an effort of NIH Common Fund's Metabolomics Data Repository and Coordinating Center supported by U2C DK119886. We thank Drs John N. Glushka and Arthur Edison for their assistance with NMR spectroscopy. RKL is supported by the Walter G Ross Foundation.

References

1 U. Schlotzer-Schrehardt and G. O. Naumann, Ocular and systemic pseudoexfoliation syndrome, *Am. J. Ophthalmol.*, 2006, **141**, 921–937, DOI: 10.1016/j.ajo.2006.01.047.

2 R. Ritch and U. Schlotzer-Schrehardt, Exfoliation syndrome, *Surv. Ophthalmol.*, 2001, **45**, 265–315, DOI: 10.1016/s0039-6257(00)00196-x.

3 K. Tekin, M. Inanc and U. Elgin, Monitoring and management of the patient with pseudoexfoliation syndrome: current perspectives, *Clin. Ophthalmol.*, 2019, **13**, 453–464, DOI: 10.2147/OPTH.S181444.

4 H. Forsius, E. Forsman, J. Fellman and A. W. Eriksson, Exfoliation syndrome: frequency, gender distribution and association with climatically induced alterations of the cornea and conjunctiva, *Acta Ophthalmol. Scand.*, 2002, **80**, 478–484, DOI: 10.1034/j.1600-0420.2002.800504.x.

5 L. Caporali, *et al.*, Incomplete penetrance in mitochondrial optic neuropathies, *Mitochondrion*, 2017, **36**, 130–137, DOI: 10.1016/j.mito.2017.07.004.

6 K. F. Damji, *et al.*, Is pseudoexfoliation syndrome inherited? A review of genetic and nongenetic factors and a new observation, *Ophthalmic Genet.*, 1998, **19**, 175–185, DOI: 10.1076/opge.19.4.175.2310.

7 R. R. Allingham, *et al.*, Pseudoexfoliation syndrome in Icelandic families, *Br. J. Ophthalmol.*, 2001, **85**, 702–707, DOI: 10.1136/bjo.85.6.702.

8 J. G. Hardie, F. Mercieca, T. Fenech and A. Cuschieri, Familial pseudoexfoliation in Gozo, *Eye*, 2005, **19**, 1280–1285, DOI: 10.1038/sj.eye.6701767.

9 A. C. Orr, *et al.*, Exfoliation syndrome: clinical and genetic features, *Ophthalmic Genet.*, 2001, **22**, 171–185, DOI: 10.1076/opge.22.3.171.2223.

10 I. F. Aboobakar and R. R. Allingham, Genetics of exfoliation syndrome and glaucoma, *Int. Ophthalmol. Clin.*, 2014, **54**, 43–56, DOI: 10.1097/IIO.0000000000000042.

11 T. Aung, A. S. Chan and C. C. Khor, Genetics of Exfoliation Syndrome, *J. Glaucoma*, 2018, **27**(suppl. 1), S12–S14, DOI: 10.1097/IJG.0000000000000928.

12 S. Dewundara and L. R. Pasquale, Exfoliation syndrome: a disease with an environmental component, *Curr. Opin. Ophthalmol.*, 2015, **26**, 78–81, DOI: 10.1097/ICU.0000000000000135.

13 A. Ringvold, Epidemiology of the pseudo-exfoliation syndrome, *Acta Ophthalmol. Scand.*, 1999, **77**, 371–375, DOI: 10.1034/j.1600-0420.1999.770401.x.

14 J. Benitez-del-Castillo Sanchez, M. Morion-Grande, M. C. Marco-Garcia and T. Parron-Carreno, Epidemiology of pseudoexfoliation syndrome: demystifying legends and looking to the future, *Arch. Soc. Esp. Oftalmol.*, 2015, **90**, 455–457, DOI: 10.1016/j.oftal.2015.07.002.

15 J. H. Kang, S. Loomis, J. L. Wiggs, J. D. Stein and L. R. Pasquale, Demographic and geographic features of exfoliation glaucoma in 2 United States-based prospective cohorts, *Ophthalmology*, 2012, **119**, 27–35, DOI: 10.1016/j.ophtha.2011.06.018.

16 L. R. Pasquale, *et al.*, Solar exposure and residential geographic history in relation to exfoliation syndrome in the United States and Israel, *JAMA Ophthalmol.*, 2014, **132**, 1439–1445, DOI: 10.1001/jamaophthalmol.2014.3326.

17 F. M. Turkcu, O. G. Koz, A. Yarangumeli, V. Oner and G. Kural, Plasma homocysteine, folic acid, and vitamin B(1)(2) levels in patients with pseudoexfoliation syndrome, pseudoexfoliation glaucoma, and normotensive glaucoma, *Medicina*, 2013, **49**, 214–218.

18 H. Leibovitzh, *et al.*, Relationship between homocysteine and intraocular pressure in men and women: a population-based study, *Medicine*, 2016, **95**, e4858, DOI: 10.1097/MD.0000000000004858.

19 T. Cumurcu, S. Sahin and E. Aydin, Serum homocysteine, vitamin B 12 and folic acid levels in different types of glaucoma, *BMC Ophthalmol.*, 2006, **6**, 6, DOI: 10.1186/1471-2415-6-6.

20 S. Bleich, *et al.*, Elevated homocysteine levels in aqueous humor of patients with pseudoexfoliation glaucoma, *Am. J. Ophthalmol.*, 2004, **138**, 162–164, DOI: 10.1016/j.ajo.2004.02.027.

21 F. Zacharaki, *et al.*, Plasma homocysteine and genetic variants of homocysteine metabolism enzymes in patients from central Greece with primary open-angle glaucoma and pseudoexfoliation glaucoma, *Clin. Ophthalmol.*, 2014, **8**, 1819–1825, DOI: 10.2147/OPTH.S64904.

22 R. K. Lee, The molecular pathophysiology of pseudoexfoliation glaucoma, *Curr. Opin. Ophthalmol.*, 2008, **19**, 95–101, DOI: 10.1097/ICU.0b013e3282f49cda.

23 I. F. Aboobakar, W. M. Johnson, W. D. Stamer, M. A. Hauser and R. R. Allingham, Major review: exfoliation syndrome; advances in disease genetics, molecular biology, and

epidemiology, *Exp. Eye Res.*, 2017, **154**, 88–103, DOI: 10.1016/j.exer.2016.11.011.
24 K. Zagajewska, *et al.*, GWAS links variants in neuronal development and actin remodeling related loci with pseudoexfoliation syndrome without glaucoma, *Exp. Eye Res.*, 2018, **168**, 138–148, DOI: 10.1016/j.exer.2017.12.006.
25 M. Krumbiegel, *et al.*, Genome-wide association study with DNA pooling identifies variants at CNTNAP2 associated with pseudoexfoliation syndrome, *Eur. J. Hum. Genet.*, 2011, **19**, 186–193, DOI: 10.1038/ejhg.2010.144.
26 S. Sharma, *et al.*, Novel protein constituents of pathological ocular pseudoexfoliation syndrome deposits identified with mass spectrometry, *Mol. Vision*, 2018, **24**, 801–817.
27 U. Schlotzer-Schrehardt, Genetics and genomics of pseudoexfoliation syndrome/glaucoma, *Middle East Afr. J. Ophthalmol.*, 2011, **18**, 30–36, DOI: 10.4103/0974-9233.75882.
28 J. Y. Chang, *et al.*, Role of nitric oxide in murine conventional outflow physiology, *Am. J. Physiol.: Cell Physiol.*, 2015, **309**, C205–C214, DOI: 10.1152/ajpcell.00347.2014.
29 H. Lu, *et al.*, Complex interactions of Tyrp1 in the eye, *Mol. Vision*, 2011, **17**, 2455–2468.
30 H. H. Mark, Aqueous humor dynamics in historical perspective, *Surv. Ophthalmol.*, 2010, **55**, 89–100, DOI: 10.1016/j.survophthal.2009.06.005.
31 M. M. Civan and A. D. Macknight, The ins and outs of aqueous humour secretion, *Exp. Eye Res.*, 2004, **78**, 625–631.
32 D. F. Cole, Secretion of the aqueous humour, *Exp. Eye Res.*, 1977, **25**(supp. l), 161–176.
33 D. F. Cole, in *The Eye – Vegetative physiology and biochemistry*, ed. H. Davson, Academic Press, 1984, vol. 1A.
34 A. Bill, The role of ciliary blood flow and ultrafiltration in aqueous humor formation, *Exp. Eye Res.*, 1973, **16**, 287–298.
35 M. J. Margolis, M. Martinez, J. Valencia, R. K. Lee and S. K. Bhattacharya, Phospholipid secretions of organ cultured ciliary body, *J. Cell. Biochem.*, 2018, **119**, 2556–2566, DOI: 10.1002/jcb.26419.
36 R. L. Cooper, I. J. Constable and L. Davidson, Aqueous humor catecholamines, *Curr. Eye Res.*, 1984, **3**, 809–813.
37 A. Bill, Uveoscleral drainage of aqueous humor: physiology and pharmacology, *Prog. Clin. Biol. Res.*, 1989, **312**, 417–427.
38 A. Bill and C. I. Phillips, Uveoscleral drainage of aqueous humour in human eyes, *Exp. Eye Res.*, 1971, **12**, 275–281.
39 M. Johnstone, E. Martin and A. Jamil, Pulsatile flow into the aqueous veins: manifestations in normal and glaucomatous eyes, *Exp. Eye Res.*, 2011, **92**, 318–327.
40 M. A. Johnstone, The aqueous outflow system as a mechanical pump: evidence from examination of tissue and aqueous movement in human and non-human primates, *J. Glaucoma*, 2004, **13**, 421–438, DOI: 10.1097/01.ijg.0000131757.63542.24.
41 M. Johnson, What controls aqueous humour outflow resistance?, *Exp. Eye Res.*, 2006, **82**, 545–557, DOI: 10.1016/j.exer.2005.10.011.
42 B. A. Boughton, *et al.*, Detection of small molecule concentration gradients in ocular tissues and humours, *J. Mass Spectrom.*, 2019, **42**, 1–14, DOI: 10.1002/jms.4460.
43 M. Tosun, M. Erdurmus, G. Bugdayci, S. Celebi and A. Alcelik, Aqueous humour and serum concentration of asymmetric dimethyl arginine in pseudoexfoliation syndrome, *Br. J. Ophthalmol.*, 2012, **96**, 1137–1140, DOI: 10.1136/bjophthalmol-2012-301901.
44 A. Eldar, *et al.*, Partial penetrance facilitates developmental evolution in bacteria, *Nature*, 2009, **460**, 510–514, DOI: 10.1038/nature08150.
45 H. Han and X. Jiang, Overcome support vector machine diagnosis overfitting, *Cancer Inf.*, 2014, **13**, 145–158, DOI: 10.4137/CIN.S13875.
46 H. Kotikoski, E. Moilanen, H. Vapaatalo and E. Aine, Biochemical markers of the L-arginine-nitric oxide pathway in the aqueous humour in glaucoma patients, *Acta Ophthalmol. Scand.*, 2002, **80**, 191–195, DOI: 10.1034/j.1600-0420.2002.800214.x.
47 A. Piotrowska, J. Wierzbicka and M. A. Zmijewski, Vitamin D in the skin physiology and pathology, *Acta Biochim. Pol.*, 2016, **63**, 17–29, DOI: 10.18388/abp.2015_1104.
48 M. Fris, J. Cejkova and A. Midelfart, Changes in aqueous humour following single or repeated UVB irradiation of rabbit cornea, *Graefes. Arch. Clin. Exp. Ophthalmol.*, 2007, **245**, 1705–1711, DOI: 10.1007/s00417-007-0620-7.
49 Y. Lin, *et al.*, Enhancement of vitamin D metabolites in the eye following vitamin D3 supplementation and UV-B irradiation, *Curr. Eye Res.*, 2012, **37**, 871–878, DOI: 10.3109/02713683.2012.688235.
50 M. R., Jr. Lattimore, Effect of ultraviolet radiation on the energy metabolism of the corneal epithelium of the rabbit, *Photochem. Photobiol.*, 1989, **49**, 175–180, DOI: 10.1111/j.1751-1097.1989.tb04093.x.
51 A. A. Kliuchnikova, *et al.*, Human aqueous humor proteome in cataract, glaucoma, and pseudoexfoliation syndrome, *Proteomics*, 2016, **16**, 1938–1946, DOI: 10.1002/pmic.201500423.
52 A. Botling Taube, A. Konzer, A. Alm and J. Bergquist, Proteomic analysis of the aqueous humour in eyes with pseudoexfoliation syndrome, *Br. J. Ophthalmol.*, 2019, **103**, 1190–1194, DOI: 10.1136/bjophthalmol-2017-310416.
53 A. B. Taube, *et al.*, Proteins in aqueous humor from cataract patients with and without pseudoexfoliation syndrome, *Eur. J. Mass Spectrom.*, 2012, **18**, 531–541, DOI: 10.1255/ejms.1208.
54 E. Hardenborg, *et al.*, Protein content in aqueous humor from patients with pseudoexfoliation (PEX) investigated by capillary LC MALDI-TOF/TOF MS, *Proteomics Clin Appl*, 2009, **3**, 299–306, DOI: 10.1002/prca.200780077.
55 S. K. Bhattacharya, R. K. Lee, F. H. Grus and Seventh, A. P. O. R. I. C. W. G., Molecular biomarkers in glaucoma, *Invest. Ophthalmol. Visual Sci.*, 2013, **54**, 121–131, DOI: 10.1167/iovs.12-11067.
56 Z. Zhou, D. Alvarez, C. Milla and R. N. Zare, Proof of concept for identifying cystic fibrosis from perspiration samples, *Proc. Natl. Acad. Sci. U. S. A.*, 2019, **116**, 24408–24412, DOI: 10.1073/pnas.1909630116.
57 Y. Guo, H. Yu, D. Chen and Y. Y. Zhao, Machine learning distilled metabolite biomarkers for early stage renal injury, *Metabolomics*, 2019, **16**, 4, DOI: 10.1007/s11306-019-1624-0.
58 D. Tsoukalas, *et al.*, Targeted Metabolomic Analysis of Serum Fatty Acids for the Prediction of Autoimmune Diseases,

Front. Mol. Biosci., 2019, **6**, 120, DOI: 10.3389/fmolb.2019.00120.

59 M. G. Anderson, K. J. Meyer, A. Hedberg-Buenz and J. H. Fingert, Update on Animal Models of Exfoliation Syndrome, *J. Glaucoma*, 2018, **27**(suppl. 1), S78–S82, DOI: 10.1097/IJG.0000000000000911.

60 S. Ravanbakhsh, *et al.*, Accurate, fully-automated NMR spectral profiling for metabolomics, *PLoS One*, 2015, **10**, e0124219, DOI: 10.1371/journal.pone.0124219.

61 A. Le Guennec, F. Tayyari and A. S. Edison, Alternatives to Nuclear Overhauser Enhancement Spectroscopy Presat and Carr-Purcell-Meiboom-Gill Presat for NMR-Based Metabolomics, *Anal. Chem.*, 2017, **89**, 8582–8588, DOI: 10.1021/acs.analchem.7b02354.

62 E. S. Nakayasu, *et al.*, MPLEx: a Robust and Universal Protocol for Single-Sample Integrative Proteomic, Metabolomic, and Lipidomic Analyses, *mSystems*, 2016, **1**(3), e00043-16, DOI: 10.1128/mSystems.00043-16.